

Extended summary

## Analysis of the problems in the FSW of advanced light alloys

*Curriculum: Ingegneria meccanica e Gestionale XII° ciclo*

Author

Giovanni Quercetti

Tutor

Prof. S. Spigarelli

Date: 20-01-2014



## 1 Problem statement and objectives

FSW produces joints by plunging the pin at the bottom of the rotating tool into the workpiece and traversing it along the joint to cause bonding by stirring and mixing.

As a solid-state welding technology, the FSW process has been proved to be a feasible technique to join dissimilar Al/Mg alloys [1–10]. Somasekharan and Murr [1] reported the friction stir weldability of magnesium alloys to 6061-T6 aluminum alloy. The weld zone showed a defect-free dissimilar weld, but the microhardness distribution in the weld was uneven, and erratic hardness spikes exhibited hardness values as much as three times those of the base material. Attempts to join Mg to Al alloys by means of FSW, however, have resulted in the formation of brittle intermetallic phases leading to poor mechanical properties for the joint [4]. It was reported that an intermetallic layer about 1  $\mu\text{m}$ -thick, consisting mainly of fine-grained  $\text{Al}_{12}\text{Mg}_{17}$ .  $\text{Al}_3\text{Mg}_2$  was rarely present and occurred in small amounts as nano-sized inclusions close to the interface, sometimes attached to the fine-grained  $\text{Al}_{12}\text{Mg}_{17}$  but rarely directly to the AZ31 alloy. In this regard, in the butt welding of 6061 to AZ31, the intermetallic layer at the Al/Mg interface was reported to be  $\text{Al}_3\text{Mg}_2$ , as identified by Firouzdor et al. [5], using EPMA or EDX techniques.

To complicate the microstructure modification at the stir welded zone, small amounts of discontinuous oxide films can also form and remain after FSW at the former Al/Mg interface. The solid-state nature and relatively lower temperature of the process compared to fusion welding processes, make FSW a potential technique for joining dissimilar materials with reasonably good joint strength. This is due to the fact that FSW potentially ensures a limited amount of rather thin brittle intermetallic compounds at the Al–Mg dissimilar weld interface. In addition, thin and discontinuous oxide films can form along the weld interface.

In this first part, the present paper aims to investigate the microstructure and the high temperature mechanical properties, using creep experiments, in a bimetallic AZ31+AA6061 friction stir welded joint.

In the second part the present paper, aims to find the friction stir welding conditions for a lap joint, in terms of process parameters, tool geometry and surface state, with which to realize AA5754 aluminum alloy blank assemblies characterized by different thicknesses. Different are the joint configurations available in literature, such as the butt joint, the lap or overlapping joint, the t-shaped joint, the hybrid lap-butt joints as reported by Li and Shen [11] even though, among them, the most studied are the butt joint and the lap joint configurations.

Among the friction stir welding configurations the most studied is the butt joint. For example, Yang et al. [12] studied the friction stir lap welding of magnesium alloys with different probe and shoulder geometries and evidenced the hook formation in both the advancing and the retreating sides. Such hook formation could represent an evidence of the vertical material flow required in the friction stir lap welding in order to supply a welded joint. In particular, the vertical flow could be increased using a threaded tool as already reported by Trimble et al. [13], even though that kind of tool is subjected to material sticking and wear. X. Cao et al. [14] reported that, in order to obtain an increased nugget depth, the probe should be longer than the thickness of the higher thicker sheet. A numerical model was built by Buffa et al. [15] for friction stir welding under overlapping configuration for blanks with same thicknesses in order to analyze the effect of the process parameters and of the tool geometry on material flow, taking into account the extension of the welding area. Under lap conditions, the method to check the strength of the joint is represented by the tensile-shear test in which the joint is nominally subjected to shear as reported by Yang et al. [12].

In the present investigation, the effect of the rotational velocity of the tool, of the welding velocity and of the tool geometry on the strength of joints realized with the friction stir welding of overlapped sheets with thickness of 3 and 1.5 mm, respectively, has been investigated. In particular, concerning the tool geometry a concave shoulder was considered with two probe configurations: the thick probe and the slender probe. It has been observed an evident effect of the welding velocity on the strength of the joint. Also to match productivity requirements, the welding velocity has been increased for both the tool configurations. It was observed that, notwithstanding the slender probe allows the welding at least up to 10 mm/min, the tractioned welded blanks show a configuration typical of stuck elements with an increased grain size. It was also found that the oxide layer at the blank to blank interface has a negligible effect on the tensile-shear strength of the joint and does not vary the macrostructure.

## 2 Research planning and activities

### 2.1 High temperature plasticity of bimetallic magnesium and aluminum friction stir welded joints

The materials investigated in the present study, the AA6061-T4 and AZ31B alloys were provided in the form of 3.2 mm-thick, 200 mm x 100 mm plates. The AZ31 alloy had an initial recrystallized microstructure, with an average grain size close to 10  $\mu\text{m}$ . The plates were butt-welded using a VA65II SEIKI CNC milling machine. A threaded H-13 steel welding tool was used in this work; the tool consisted of a 3 mm high-threaded conic pin having a diameter of 6.3 mm at its base and 4.5 mm at its edge, and a 20 mm diameter shoulder. The welding direction was perpendicular to the rolling direction of the materials. The pin was inclined with respect to the plates with an angle set at 3°. All the welded specimens were examined by a low-magnification optical microscope. The optimal welding parameters were found to be a rotational speed of 800 rpm and a transverse pin speed of 5 mm/min with the Mg plate at the advancing side and a 1.5 mm offset of the welding tool into the Mg side. FSW sections were polished and prepared by a two-step etching procedure. In the first step an etching solution consisting of 10 mL acetic acid, 10 mL distilled water, and 6 g picric acid in 100 mL ethanol was used for 10 s, in order to reveal the AZ31 microstructure. In the second step, a solution consisting of 20 g NaOH in 100 mL distilled water was used for 40 s, to reveal the AA6061 grained structure.

The overview inspections were carried out using a Reichert Joug MeF3 light-microscope. The detailed microstructure analyses were performed using a Zeiss Supra 40 FEGSEM and equipped with an EDS facility for the qualitative elemental chemical analyses of the intermetallic compounds. Microhardness tests were performed using a Remet HX1000 with a 200 g load. Constant load creep experiments at 473 K were carried out on samples, with 3 mm x 3 mm section and 25 mm gauge length.

### 2.2 Friction stir lap welding of blanks with different tool configurations

The friction stir welding tests were performed in a machining center. The sheets in AA 5754 aluminum alloy were respectively 3 and 1.5 mm in thickness. The welding was performed under the overlapping configuration. The tool used for friction stir welding was in h13 steel.

The welding parameters considered were the rotational velocity and the welding velocity. The tilt angle, was considered equal to 2°. Two kinds of tool characterized by the same

shoulder with a diameter of 20 mm, but with two probe configurations as reported in figure 1.

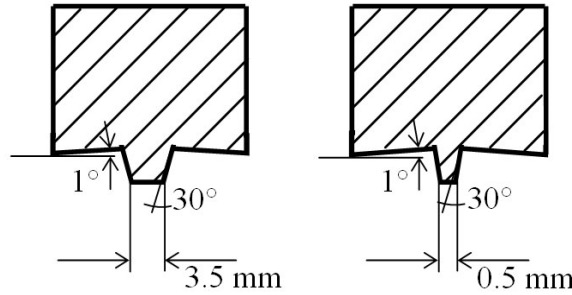


Figure 1 Tools with thick and slender probes.

A full  $2^k$  factorial design with  $k=3$  factors, that are the rotational velocity of the tool ( $\alpha$ ), the welding velocity ( $\beta$ ) and the tool configuration ( $\chi$ ), was considered. In particular  $\alpha$  and  $\beta$  were varied between 1 and 5 mm/min and between 2000 and 2500 rev/min, respectively. Whilst,  $\chi$  was varied between the thick and slender tool configuration. The response was the tensile-shear strength of the welded joints. The analysis of variance was applied and the effect of the factors evaluated.

In particular the effects of  $\alpha$ ,  $\beta$ ,  $\chi$ ,  $\alpha\beta$ ,  $\beta\chi$ , and  $\alpha\beta\chi$  were calculated using the following equation:

$$Effect = [contr] / n2^{k-1}$$

where *contr* is the contrast, evaluated from the table 1, for instance as:

$$contr_{\alpha} = [-(1) + \alpha - \beta + \alpha\beta - \chi + \alpha\chi - \chi\beta + \alpha\beta\chi]$$

and  $n$  the number of replications, with  $n=2$ , for each condition in terms of  $\alpha$ ,  $\beta$ ,  $\chi$  reported in table 1. The sums of squares were calculated as:

$$SS = [contr]^2 / n2^k \text{ the total sum of squares as:}$$

$$SS_{total} = \sum_{i=1}^{\alpha} \sum_{j=1}^{\beta} \sum_{k=1}^{\chi} \sum_{z=1}^n y_{ijkz}^2 - \left( \sum_{i=1}^{\alpha} \sum_{j=1}^{\beta} \sum_{k=1}^{\chi} \sum_{z=1}^n y_{ijkz} \right)^2 / \alpha\beta\chi n \text{ the sum of squares of error as:}$$

$$SS_{error} = SS_{total} - SS_{\alpha} - SS_{\beta} - SS_{\chi} - SS_{\alpha\beta} - SS_{\beta\chi} - SS_{\alpha\chi} - SS_{\alpha\beta\chi} \text{ the mean squares as:}$$

$$MS = SS / d.o.f. , \text{ where d.o.f. represents the degrees of freedom.}$$

The F test was performed considering that:

$$F = MS_{\alpha, \beta, \chi, \alpha\beta, \beta\chi, \alpha\chi, \alpha\beta\chi} / MS_{res}$$

The influence of the superficial oxide layer on the tensile-shear strength and on the integrity of the transversal area of the joints was also investigated in which the superficial oxide layer was previously mechanically ground.

Table 1. Experimental design for the friction stir welding operations performed, with the oxide layer, in the following conditions:  $\alpha$  (-1: 2000 rev/min, +1: 2500 rev/min);  $\beta$  (-1: 1 mm/min, +1: 5 mm/min);  $\chi$  (-1: thick tool, +1: 3 slender tool).

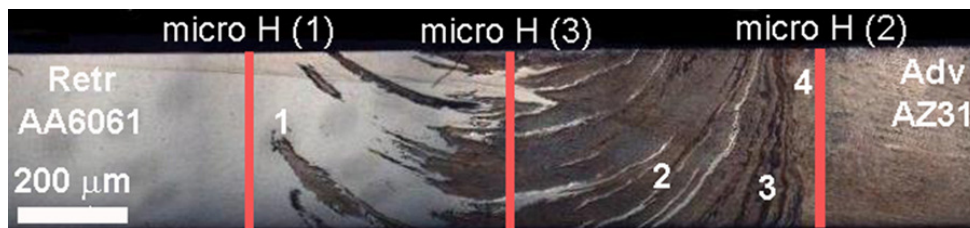
	Rotational velocity of the tool, rev/min ( $\alpha$ )	Welding velocity, mm/min ( $\beta$ )	Type of tool ( $\chi$ )
(1)	-1	-1	-1
$\alpha$	1	-1	-1
$\beta$	-1	1	-1
$\alpha\beta$	1	1	-1
$\chi$	-1	-1	1
$\alpha\chi$	1	-1	1
$\chi\beta$	-1	1	1
$\alpha\beta\chi$	1	1	1

### 3 Analysis and discussion of main results

#### 3.1 High temperature plasticity of bimetallic magnesium and aluminum friction stir welded joints

##### 3.1.1 Microstructure of the as-welded joint

Figure 2 reports an FSW overview at the top view of the joined plates, figure 2(a), and some detailed zones in the stirring zone of the dissimilar Al/Mg welded plates, figure 2(b) to (e). The AZ31 alloy is pushed upward, due to the continuous downward flow imposed by the rotating pin, figure 2(a). As a result, some of the detached magnesium alloy particles, on the Al side, and some of the detached aluminum alloy strings (the white portions in the micrographs), on the Mg side, are moved away from the bonding line, figure 2(b) and (c). The chemical reaction and diffusion between the transported AZ31 alloy and the AA6061 alloy lead to the formation of the thin strips of intermetallic compounds observed in figure 2(d). From figure 2 it is also apparent that the interfacial region of dissimilar joints produced by FSW undergoes complex deformation associated with high heating and high cooling rates. Fine-grained microstructures characterize the nugget zone (WNZ, Figure 2(e)), where new phases appear as a result of solid-state reactions.



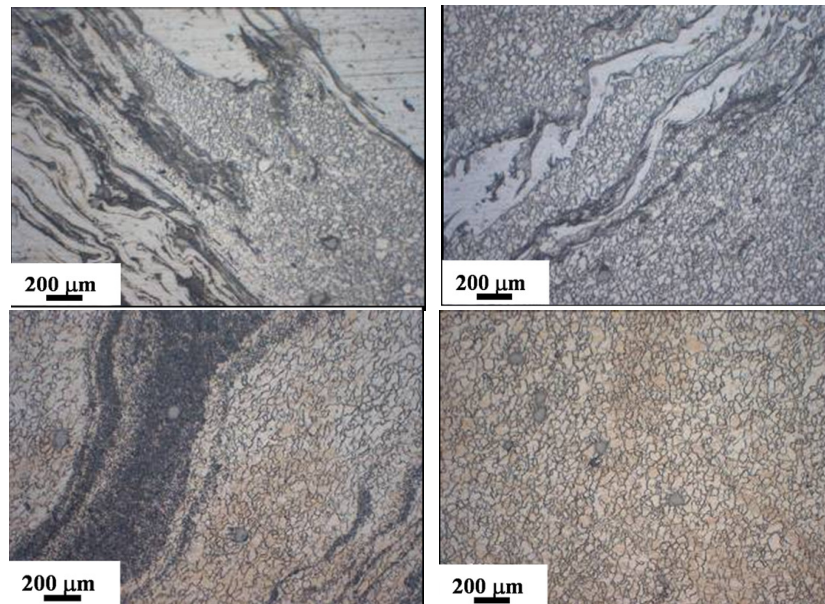


Figure 2 a) LM images showing the top surface macrostructure across the FSW stirred zone, and the location of the three microhardness profiles; b) and c) are detailed of zones 1 and 2 of a). d) Shows intermetallic compounds strip at the Al/Mg interface layers (zone 3 of a)). E) Shows the nugget grained structure consisting of CDRX Mg grains (zone 4 of a)).

FEGSEM EDS analyses allowed the existing new phases at the AZ31/AA6061 interface to be identified as intermetallic compounds, whose chemical nature is fully consistent with the  $\text{Al}_{12}\text{Mg}_{17}$  and  $\text{Al}_3\text{Mg}_2$  phases (figure 3).

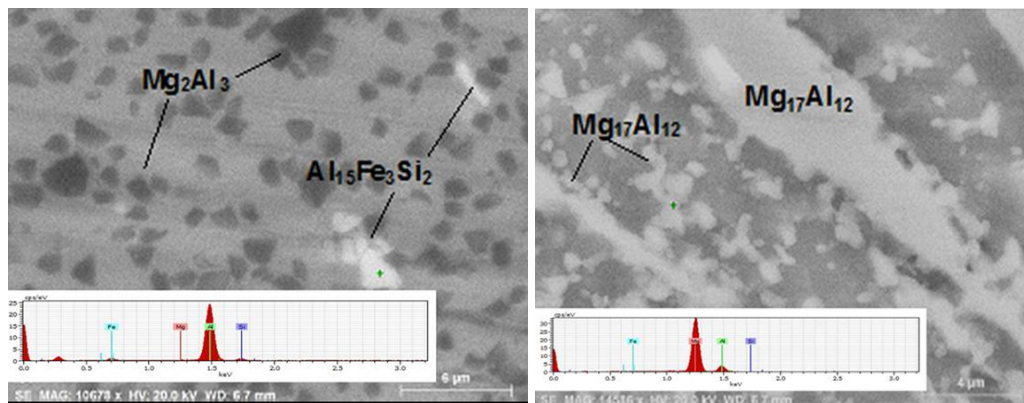


Figure 3 Back-scattered FEGSEM image of the top interface region between AA6061 and AZ31: a) refers to the Al side, while, b) refers to the Mg side.

### 3.1.2 Creep results: Quantification of strain localization by an analytical procedure

Figure 4 shows the cumulative strain distribution measured along the gauge length after creep testing; it can easily be appreciated that, while under the lowest stress, deformation is almost homogeneously distributed in the Mg-containing portion of the sample, while under high stresses the deformation becomes more and more localized. Figure 5 il-

illustrates more clearly that deformation is concentrated in the part of the sample (zone II) which roughly corresponds to the WNZ; a lower but not negligible deformation is also observed in zone I and in zone III. No deformation is observed in zone IV. Zone I is composed of AZ31 magnesium alloy, i.e. the magnesium base metal, the heat affected zone and part of the TMAZ; zone II is the most deformable part, and is composed of the rest of the TMAZ and most of the WNZ; zone III is composed of the TMAZ (aluminum side), but still contains a high fraction of Mg; zone IV is the undeformed Al alloy.

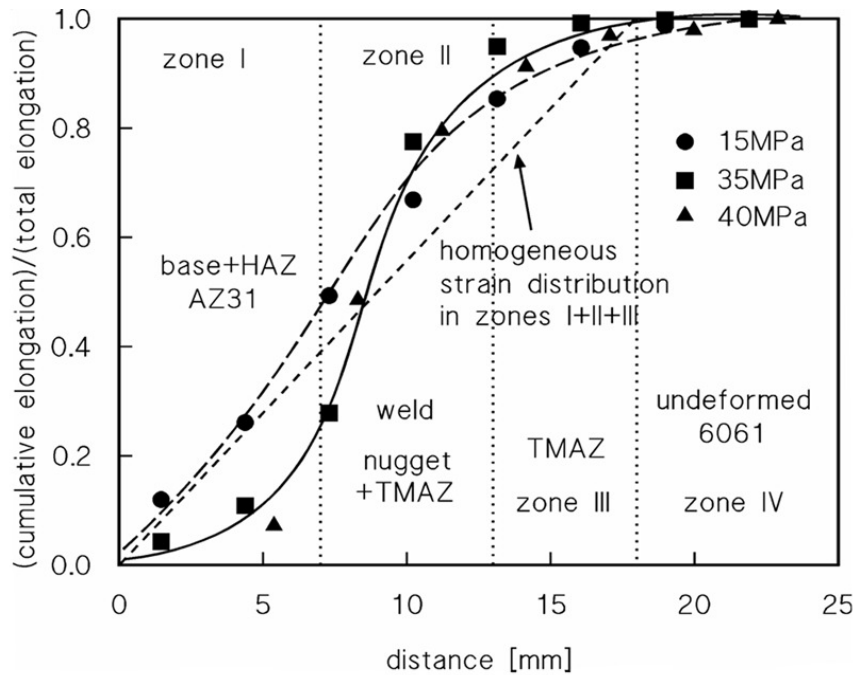


Figure 4 Cumulative strain distribution along the gauge length of the cross weld FSW creep samples after mechanical testing under constant load at 200°C.

Figure 5 also presents the straight line which corresponds to a homogeneous strain in zones I, II and III, and an approximated model describing the experimental strain distribution.

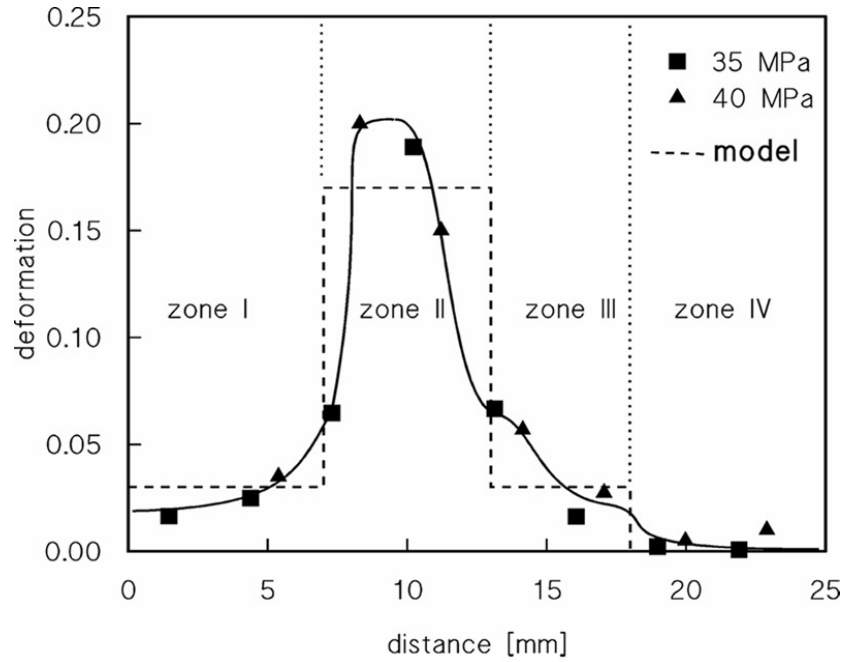


Figure 5 Experimental and modeled strain distribution along the gauge length of the crept samples.

A simplified description of the creep response of the cross-weld samples can be attempted by considering that the gauge length is composed of the 4 zones shown in figure 9, which also reports a simplified strain distribution (broken line). The overall strain can thus be approximately calculated as:

$$\varepsilon_{cw} = \sum f_i \varepsilon_i \quad (1)$$

where  $f_i$  and  $\varepsilon_i$  are the volume fraction and the local strain in the  $i$ -component. Since zones I and III deform to a similar extent, they will be modeled as a single constituent, which behaves like the base AZ31. Thus, the total strain will have the form:

$$\varepsilon_{cw} = f_{bMg} \varepsilon_{bMg} + f_w \varepsilon_w + f_{bAl} \varepsilon_{bAl} \quad (2)$$

where the suffixes bMg, w and Al indicate the materials of zones (I+III), II and IV respectively. A good estimate of the  $\varepsilon_{bMg}$  component can be obtained in all those cases in which the creep curve, under the same experimental condition, is available for the base AZ31 alloy. Since  $\varepsilon_{Al} \cong 0$ , the strain in zone II at time  $t$  can thus be calculated as:

$$\varepsilon_w(t) = \frac{\varepsilon_{cw}(t) - f_{bMg} \varepsilon_{bMg}(t)}{f_w} \quad (3)$$

An example of this procedure is shown in figure 6. The values of  $f_{bMg}$  and  $f_w$  were obtained by considering the simplified strain distribution in figure 5. The  $\varepsilon_w$  vs.  $t$  curve obtained by this procedure can be used to calculate the  $\varepsilon_w / \varepsilon_{bMg}$  ratio at the rupture of the cross-weld sample (figure An example of this procedure is shown in figure 6. The values of  $f_{bMg}$  and  $f_w$  were obtained by considering the simplified strain distribution in figure 5.

The  $\epsilon_w$  vs.  $t$  curve obtained by this procedure can be used to calculate the  $\epsilon_w/\epsilon_{bMg}$  ratio at the rupture of the cross-weld sample and the minimum strain rate in zone II.

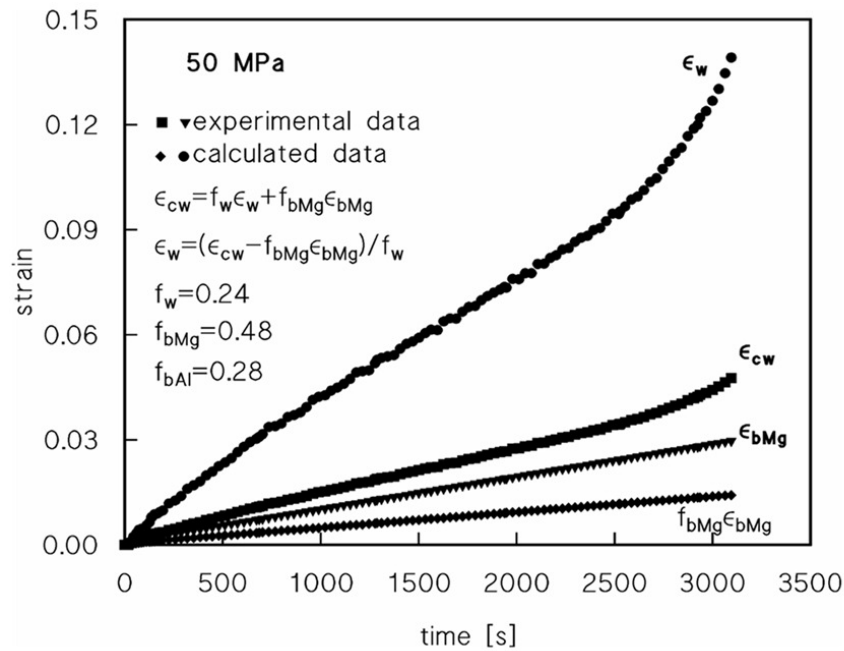


Figure 6 Creep for the weld zone calculated following the procedure illustrated in the text.

### 3.2 Friction stir lap welding of blanks with different tool configurations: Analysis and discussion

The results obtained from tensile-shear testing of the welded sheets are reported in table 2. The result of the analysis of variance evidences, as reported in table 3.

Table 2 results given by the experimental design for the friction stir welding operations performed with the following conditions:  $\alpha$  (-1: 2000 rev/min, +1: 2500 rev/min);  $\beta$  (-1: 1 mm/min, +1: 5 mm/min);  $\chi$  (-1: thick tool, +1: 3 slender tool).

	Rotational velocity of the tool, rev/min ( $\alpha$ )	Welding velocity, mm/min ( $\beta$ )	Type of tool ( $\chi$ )	Strength of the joint, kN/mm	
(1)	-1	-1	-1	0,337	0,3333
$\alpha$	1	-1	-1	0,33	0,2966
$\beta$	-1	1	-1	0,285	0,21
$\alpha\beta$	1	1	-1	0,263	0,2558
$\chi$	-1	-1	1	0,322	0,3233
$\alpha\chi$	1	-1	1	0,285	0,3225
$\chi\beta$	-1	1	1	0,198	0,225
$\alpha\beta\chi$	1	1	1	0,263	0,2766

Table 3 results of the analysis of variance for friction stir welding operations performed with the following conditions:  $\alpha$  (-1: 2000 rev/min, +1: 2500 rev/min);  $\beta$  (-1: 1 mm/min, +1: 5 mm/min);  $\chi$  (-1: thick tool, +1: 3 slender tool)

	Effects	sums of squares, SS	d.o.f.	Mean squares, M.S.	F
$\alpha$	0,00723	0,0002	1	0,0002	0,3658
$\beta$	-0,0717	0,0205	1	0,0205	35,9026
$\chi$	-0,0118	0,0005	1	0,0005	0,9756
$\alpha\beta$	0,0277	0,0030	1	0,0030	5,3791
$\beta\chi$	-0,0010	4,79E-06	1	4,79E-06	0,0083
$\alpha\chi$	0,0125	0,0006	1	0,0006	1,0815
$\alpha\beta\chi$	0,0109	0,0004	1	0,0004	0,8270
Sum of squares of error, $SS_{error}$		0,0045	8	0,0005	
Total sum of squares, $SS_{total}$		0,0301	15		

Taking into consideration the results reported in table 3, the study was subsequently oriented towards more elevated welding velocities, in particular at the 2500 rev/min. For such reason further welding tests were performed at 2500 rev/min with both the tool typologies considered in the present study. The welding velocity was increased up to 10 mm/min. The welding results were reported in figures 7 and 8. In particular, figure 7 shows the decrease in the tensile-shear strength with increasing welding velocities for both tool typologies utilized. For the slender tool at the highest welding velocity investigated of 10 mm/min, the specimens after tensile-shear tests appear stuck together instead of welded, as reported in figure 8.

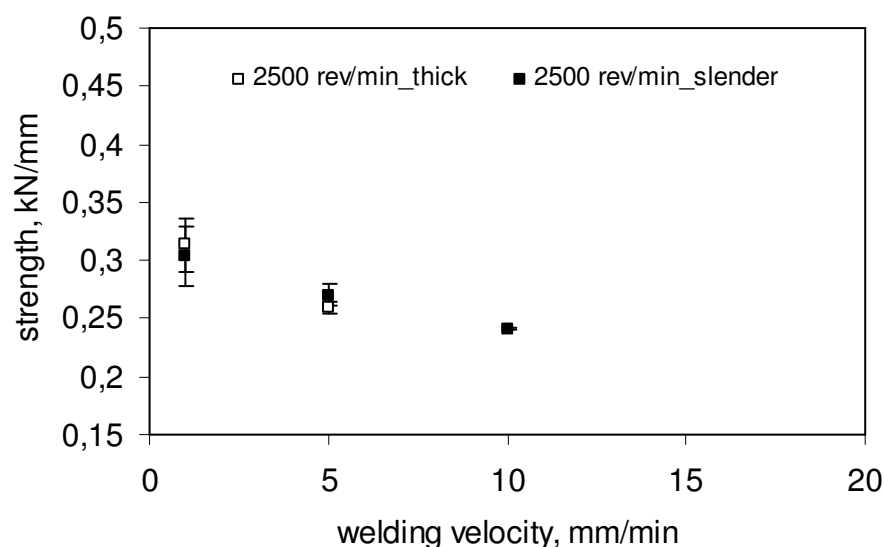


Figure 7 Tensile-shear strength vs. welding velocity at 2500 rev/min for joints obtained with thick tool and with slender tool with welding velocities up to 10 mm/min.

In order to investigate the possibility to increase the tensile-shear strength of the joints obtained at 2500 rev/min with both the thick and the slender tools, at more elevated welding velocities, the surfaces of the blanks were mechanically ground before welding with the end to eliminate the oxide layer.



Figure 8 Typical configuration of the tractioned specimen obtained under welding conditions of 2500 rev/min with the welding velocity of 10 mm/min for the slender tool.

The tensile-shear strength of the joints, obtained under slender tool conditions, were plotted and compared to each other, under two configurations: the welded blanks obtained without eliminating the oxide layer at the interface and the welded blanks obtained eliminating the oxide layer at the interface, as reported in figure 9.

However, the thermal exposure could have a relatively low or high impact on the grain size of the welded joints depending on the welding parameters that determined the heat generated. The stirring zone is characterized by dynamically recrystallized grains due to the in temperature plastic deformation taking place by means of the tool probe. The typical zone distribution already reported is in agreement with that found by Mishra and Ma [16].

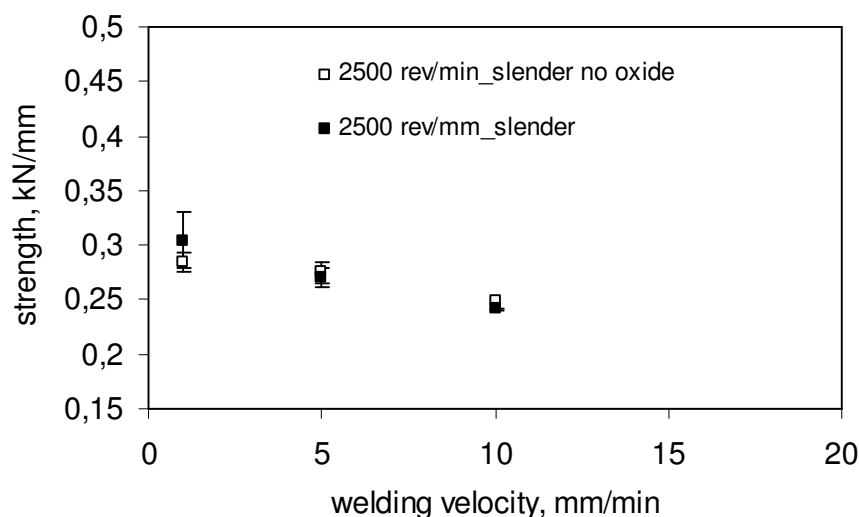


Figure 9 Tensile-shear strength vs. welding velocity, up to 10 mm/min, for specimens obtained from welded sheets at 2500 rev/min through the slender tool with and without the oxide layer on the surfaces.

#### 4 Conclusions

The high temperature deformation at 473 K of a bimetallic AZ31/AA6061 Friction Stir Welded joint was investigated by constant load creep experiments. The analysis of the experimental data revealed that the AA6061 alloy, in the investigated range of stress, did not undergo significant creep strain. Both analytical and experimental calculations demonstrated that deformation, in the high stress regime, was concentrated in the weld zone, characterized by a strongly refined grain size in the magnesium-rich portion of the joint. In the low stress region, deformation became more and more homogeneously distributed in the sample, with the exception of the AA6061 base metal, which remained undeformed. The experimental behavior was described by the same constitutive equation which was found to describe the high temperature response of the AZ31 alloy, modified only to take into account the role of intermetallic particles in the weld zone, which retard grain growth and obstruct grain boundary sliding.

The research activity performed consists in the friction stir welding of overlapped sheets in AA5754 aluminium alloy, with different thicknesses, of 1.5 and 3 mm respectively. The effects of the rotational velocity of the tool, of the welding velocity, and of the tool geometry on the tensile-shear strength of joints realized was quantified following a factorial design. The obtained data were analysed and it was found that, among the welding parameters, the welding velocity represents the factor that largely affects the tensile-shear strength of the friction stir welded joints. Taking a look the microstructure of the obtained joints, it was observed that the thick tool determines an increase in nugget zone with respect to that obtained with the slender tool. Such aspect has a beneficial effect, in particular at the lowest rotational velocity of the tool, on the tensile-shear strength of the friction stir welded joints. Subsequently, the welding velocity was increased up to 10 mm/min for both the tool configurations and it was observed that, notwithstanding the slender tool allows the welding at least up to 10 mm/min, the tractioned welded joints show a configuration typical of stuck elements. Furthermore, the increase in the welding velocity determines an increase in the grain size. Subsequently, the surface of the blanks, prior to welding, were mechanically ground in order to eliminate the oxide layer. Such treatment, under the conditions of the present investigation, shows a negligible effect on the tensile-shear strength of the joint.

#### References

- [1] A.C. Somasekharan, L.E. Murr: J. *Characterization of complex, solid-state flow and mixing in the friction-stir welding (FSW) of aluminum alloy 6061-T6 to magnesium alloy AZ91D using color metallography*. Mater. Sci., vol. 41, pp. 5365-70, 2006.
- [2] C. Liu, D.L. Chen, S. Bhole, X. Cao, M. Jahazi. *Polishing-assisted galvanic corrosion in the dissimilar friction stir welded joint of AZ31 magnesium alloy to 2024 aluminum alloy*. Mater. Charact., vol. 60, pp. 370-6, 2009.
- [3] P. Venkateswaran, Z.-H. Xu,, X.D. Li, A.P. Reynolds. *Determination of mechanical properties of Al-Mg alloys dissimilar friction stir welded interface by indentation methods*. J. Mater. Sci., vol. 44, pp. 4140-7.22, 2009.
- [4] Y.S. Sato, S.H.C. Park, M. Michiuchi, H. Kokawa. *FIB-assisted TEM study of an oxide array in the root of a friction stir welded aluminium alloy*. Scripta Mater., vol. 50, pp. 1233-6, 2004.

- [5] Firouzdor, V., Kou, S.. *Microstructure investigations of directionally solidified Mg-rich alloys containing Al, Ca and Sn*. Metall. Mater. Trans. A, vol. 41, pp. 3238-51, 2010.
- [6] A. Kostka, R.S. Coelho, J. dos Santos, A.R. Pyzalla. *Microstructure of friction stir welding of aluminium alloy to magnesium alloy*. Scripta Mater., vol. 60, pp. 953-6, 2009.
- [7] A.R. Yavari, P.J. Desre. *Thermodynamic and kinetic justification for amorphization by mechanical alloying of A-B metal couples with zero heat of mixing  $\Delta H_{mix}$* . Phys. Rev. Lett., vol. 65, pp. 2571-5, 1990.
- [8] G. González, A. Sagarzazu, R. Villalba, J. Ochoa. *Comparative study of NiW, NiMo and MoW prepared by mechanical alloying*. J. Alloys Compd, vols. 434–435, pp.525-9, 2007.
- [9] M.A. Mofid, A. Abdollah-zadeh, F. Malek Ghaini. *The effect of water cooling during dissimilar friction stir welding of Al alloy to Mg alloy*. Mater. & Design, vol. 36, pp.161-7, 2012.
- [10] Y.S. Sato, M. Urata, H. Kokawa. *Recovery retardation in equal channel angular pressed Al–Zr alloy during friction stir welding*. Metall. Mater. Trans. A, 2002, vol. 30, pp. 625–35.
- [11] Li, B., Shen, Y. *A feasibility research on friction stir welding of a new-typed lap–butt joint of dissimilar Al alloys*. Materials and Design 34, 725–731., 2012.
- [12] Yang, Q., Li X., Chen, K., Shi, Y.J.. *Effect of tool geometry and process condition on static strength of a magnesium friction stir lap linear weld*. Materials Science and Engineering A 528, 2463–2478, 2011.
- [13] Trimble, D., Monaghan, J., O'Donnell, G.E. *Force generation during friction stir welding of AA2024-T3*. CIRP Annals - Manufacturing Technology 61, 9–12., 2012.
- [14] Cao, X., Jahazi, M.. *Effect of tool rotational speed and probe length on lap joint quality of a friction stir welded magnesium alloy*. Materials and Design 32, 1–11., 2011.
- [15] Buffa, G., Campanile, G., Fratini, L., Prisco, A.. *Friction stir welding of lap joints: Influence of process parameters on the metallurgical and mechanical properties*. Materials Science and Engineering A 519, 19–26, 2009.
- [16] Mishra, R.S., Ma, Z.Y.. *Friction stir welding and processing*. Materials Science and Engineering R 50, 1–78., 2005.